Atmos. Chem. Phys. Discuss., 14, 16493–16528, 2014
www.atmos-chem-phys-discuss.net/14/16493/2014/
doi:10.5194/acpd-14-16493-2014

Atmospheric Chemistry and Physics Discussions
Open Access

A comprehensive parameterization of heterogeneous ice nucleation of dust surrogate: laboratory study with hematite particles and its application to atmospheric models

N. Hiranuma[1], M. Paukert[1], I. Steinke[1], K. Zhang[2], G. Kulkarni[2], C. Hoose[1], M. Schnaiter[1], H. Saathoff[1], and O. Möhler[1]

[1]Institute for Meteorology and Climate Research – Atmospheric Aerosol Research, Karlsruhe Institute of Technology, Karlsruhe, Germany
[2]Atmospheric Science and Global Change Division, Pacific Northwest National Laboratory, Richland, Washington, USA

Received: 10 May 2014 – Accepted: 16 June 2014 – Published: 24 June 2014

Correspondence to: N. Hiranuma (seong.moon@kit.edu)

Published by Copernicus Publications on behalf of the European Geosciences Union.

A comprehensive parameterization of heterogeneous ice nucleation of dust

N. Hiranuma et al.

Abstract

A new heterogeneous ice nucleation parameterization that covers a wide temperature range (−36 to −78 °C) is presented. Developing and testing such an ice nucleation parameterization, which is constrained through identical experimental conditions, is critical in order to accurately simulate the ice nucleation processes in cirrus clouds. The surface-scaled ice nucleation efficiencies of hematite particles, inferred by n_s, were derived from AIDA (Aerosol Interaction and Dynamics in the Atmosphere) cloud chamber measurements under water subsaturated conditions that were realized by continuously changing temperature (T) and relative humidity with respect to ice (RH_{ice}) in the chamber. Our measurements showed several different pathways to nucleate ice depending on T and RH_{ice} conditions. For instance, almost T-independent freezing was observed at $-60\,°C < T < -50\,°C$, where RH_{ice} explicitly controlled ice nucleation efficiency, while both T and RH_{ice} played roles in other two T regimes: $-78\,°C < T < -60\,°C$ and $-50\,°C < T < -36\,°C$. More specifically, observations at T colder than −60 °C revealed that higher RH_{ice} was necessary to maintain constant n_s, whereas T may have played a significant role in ice nucleation at T warmer than −50 °C. We implemented new n_s parameterizations into two cloud models to investigate its sensitivity and compare with the existing ice nucleation schemes towards simulating cirrus cloud properties. Our results show that the new AIDA-based parameterizations lead to an order of magnitude higher ice crystal concentrations and inhibition of homogeneous nucleation in colder temperature regions. Our cloud simulation results suggest that atmospheric dust particles that form ice nuclei at lower temperatures, below −36 °C, can potentially have stronger influence on cloud properties such as cloud longevity and initiation when compared to previous parameterizations.

ACPD
14, 16493–16528, 2014

1 Introduction

Ice clouds constitute significant source of uncertainty in predicting the Earth's climate change according to the recent Intergovernmental Panel on Climate Change 2013 report (i.e., Chapter 7 of IPCC, 2013; Boucher et al., 2013). Rare airborne particles that can act as ice nucleating particles (INPs) at supercooled temperatures indirectly influence the Earth's forcing by changing microphysical properties of ice clouds such as reflectivity, longevity and precipitation. However, understanding ice cloud formation over a wide range of atmospherically relevant temperatures and humidity is challenging (e.g., DeMott et al., 2011; Murray et al., 2012), and our knowledge of ice formation through various nucleation modes is still scarce and limited, such that the ice nucleation processes are currently very poorly represented in global climate models (e.g., Hoose et al., 2010; Liu and Penner, 2005). In particular, heterogeneous ice nucleation processes proceed through various modes including deposition nucleation, contact-, condensation- and immersion freezing (Chapter 9 of Pruppacher and Klett, 1997; Vali, 1985). Briefly, deposition mode where water vapor is directly deposited on to the INP to induce ice formation, condensation and immersion freezing can induce ice formation when freezing is initiated by the INP immersed within the supercooled droplet or solution droplet, and contact freezing can initiate at the moment when an INP comes into contact with a supercooled droplet.

A global model simulation of INPs in tropospheric clouds showed that more than 85 % of heterogeneous ice nucleation is accounted for by freezing of supercooled cloud droplets, in which INPs are either immersed or condensed (Hoose et al., 2010). However, representativeness of freezing mechanisms in cirrus clouds is still ambiguous (e.g., Sassen and Khvorostyanov, 2008). It is understood that various INPs can nucleate ice at water subsaturation and a range of supercooled temperature conditions as comprehensively illustrated in Fig. 2 of Hoose and Möhler (2012). More specifically, the potential importance of ice nucleation at ice supersaturated conditions below the homogeneous freezing threshold line (i.e., Koop line; Koop et al., 2000; Ren and MacKenzie,

ACPD
14, 16493–16528, 2014

2005) has already been proved in early studies, suggesting further investigation in the water subsaturated region. For example, Christenson (2013) experimentally showed that the capillary condensation of supercooled liquid on surface defects facilitated subsequent homogeneous nucleation and growth of ice below water saturation. Marcolli (2014) suggested that the inverse Kelvin effect below water saturation helps to form water in pores or cavities, and hypothesized that this condensate could freeze through the homogeneous- or immersion mode freezing and referred this freezing mechanism as pore condensation and freezing. Recently, Welti et al. (2014) introduced the relevance of soluble components of mineral dust (i.e., Fluka kaolinite) to condensation freezing below water saturation. Further, recent aircraft-based field observations also suggested that the dominant heterogeneous ice formation at cirrus temperatures occured at water subsaturated conditions, in particular where RH_{ice} was below 140 % (Cziczo et al., 2013). In addition, Storelvmo and Herger (2014) demonstrated that the forward modelling simulation with 50 % of mineral dust particles acting as INP to be in good agreement with an observation reported by Cziczo et al. (2013). Another airborne observation during an Asian mineral dust event also suggested ice nucleation in cirrus clouds to occur under water subsaturation conditions below 130 % RH_{ice} (Sakai et al., 2014).

Previously, empirical descriptions such as Meyers et al. (1992, henceforth M92) were derived from the limited field measurements of ice nuclei concentrations measured at $-23\,^{\circ}\mathrm{C} < T < -7\,^{\circ}\mathrm{C}$ and $102\,\% < RH_{ice} < 125\,\%$ conditions. Recently, Phillips et al. (2008, 2013) empirically parameterized the heterogeneous ice nucleation of various types of aerosol as a function of humidity ($RH_{ice} > 100\,\%$) and temperature conditions (0 to $-100\,^{\circ}\mathrm{C}$). Besides, classical nucleation theory (CNT)-based ice nucleation descriptions have also been widely used and implemented in cloud models (e.g., Barahona and Nenes, 2009a, b; Kärcher and Lohmann, 2003; Khvorostyanov and Curry, 2004). These parameterizations may predict different cloud properties for the identical environmental conditions. For example, Barahona et al. (2010) showed that the ice crystal number cloud vary up to an order of magnitude in a global chemical

ACPD
14, 16493–16528, 2014

transport model depending on the choice of the heterogeneous ice nucleation parameterization. Authors found the lowest global mean ice crystal concentration from Phillips et al. (2008) parameterization. Likewise, sensitivity of ice cloud properties to the parameterization was also observed by Liu et al. (2012). They showed that heterogeneous INP number concentration from a CNT-based parameterization was typically a few times higher than that from the Phillips's one for the identical test case conditions. Therefore, systematic laboratory measurements to develop water subsaturated ice nucleation parameterizations for the range of atmospherically relevant T-RH$_{ice}$ conditions are needed to better represent ice nucleation processes in cloud models.

Recently, Hoose and Möhler (2012) compiled previously reported aerosol-specific heterogeneous freezing efficiencies from laboratory experiments based on a single-parameter, n_s (e.g., Niemand et al., 2012; Connolly et al., 2009), and authors formulated ice nucleation efficiency by evaluating aerosol-specific "singular" freezing onsets at or after specific ambient conditions are met. Such time-independent and surface area-scaled n_s formulations cloud be further adapted to comprehensively assess the ice nucleation in a wide range of atmospherically relevant T-RH$_{ice}$ conditions. Accordingly, the n_s concept was adapted to deposition nucleation at low temperature conditions (up to −80 °C).

Herein, as part of the Ice Nucleation research UnIT (so called INUIT), we conducted a comprehensive investigations on examining the ice nucleation efficiency of pristine cubic hematite particles as a model proxy for atmospheric dust particles. Ice nucleation efficiencies of cubic hematite particles were measured using the AIDA cloud chamber. We also re-examined the previously reported AIDA results of hematite ice nucleation (Hiranuma et al., 2014; Skrotzki et al., 2013), and combined them with the results from this work in order to examine the ice nucleation efficiency of hematite particles in the temperature range between −36 and −78 °C. Applications of the fitted n_s parameterization derived from these measurements to atmospheric modeling simulations were also performed. We implemented the parameterizations in the Single column version of Community Atmospheric Model version 5 (SCAM5, Neale et al., 2010) and

ACPD
14, 16493–16528, 2014

the COnsortium for Small-scale Modeling (COSMO, Baldauf et al., 2011; Doms et al., 2011) models to assess the newly developed parameterizations and compared against existing parameterizations.

2 Method

2.1 Description of hematite particles

Laboratory-generated cubic hematite particles were used as a proxy for atmospheric dust particles. These particles had uniform composition, morphology and well defined surface area, and are therefore good to investigate and relate T-RH$_{ice}$-dependent ice nucleation efficiency to surface area (Hiranuma et al., 2014). Detailed information regarding the manufacturing process of cubic hematite particles is available elsewhere (Sugimoto and Sakata, 1992). Three different sizes of quasi-monodispersed hematite particles (∼ 200, ∼ 500 and ∼ 1000 nm diameter, respectively) were used in this work. The morphology and size of the hematite particles were characterized by scanning electron microscopy and determined based on an equivalent circle diameter derived from the observed 2-D particle projection area (Vragel, 2009; Hiranuma et al., 2014). A Small-Scale Powder Disperser (SSPD, TSI, Model 3433) was used to dry disperse the quasi-monodispersed hematite particles into the AIDA vessel.

2.2 AIDA cooling expansion

The AIDA expansion freezing experiments were achieved by mechanical pumping (Möhler et al., 2003). Mechanical pumps can be operated at different pumping speeds simulating atmospherically relevant adiabatic cooling of rising air parcels in the cylinder 84 m^3 volume (i.e., 7 m height × 4 m width) thermal conductive aluminum vessel installed inside the thermostatic housing. For this study, we typically utilized a cooling rate of 5 °C min^{-1} at the beginning, decreasing to < 0.1 °C min^{-1} within 400 s for each pumping expansion experiment, mainly due to an increasing heat flux from the chamber walls, which stay at almost constant temperature, to the stirred and well mixed volume of the cold chamber. During the experiment, the pressure in the vessel decreased from 1000 to 800 mb while pumping.

The mean gas temperature in the AIDA vessel was determined by five thermocouples deployed at different vertical levels. The sensors of these thermocouples were located about 1 m off the vessel-wall and, thus, fully exposed to the chamber air. Stirring the air by the mechanical ventilator prior to and during pumping ensured a homogeneous temperature distribution within the vessel of ±0.3 °C (Möhler et al., 2003). The relative humidities with respect to water (RH_{water}) and RH_{ice} were determined using the mean gas temperature and the mean water vapor concentration with an accuracy of ±5 %. The water vapor concentrations were measured in situ by tunable diode laser (TDL) water vapor absorption spectroscopy throughout the expansion experiments. Since this direct long path absorption technique is described and evaluated in detail in other publications (Fahey et al., 2014; Skrotzki et al., 2013), no further information are given here.

Under atmospheric pressure condition, prior to each expansion experiment, a combination of a Scanning Mobility Particle Sizer (SMPS, TSI, Model 3080 DMA and Model 3010 condensation particle counter), an Aerosol Particle Sizer (APS, TSI, Model 3321) and a condensation particle counter (CPC, TSI, Model 3076) collectively measured total number and size distribution of aerosols at the horizontally extended outlet from the AIDA chamber. Subsequently, the total aerosol surface area was estimated as presented in Hiranuma et al. (2014). During expansion, we quantified the ice nucleation of hematite particles with two different light scattering instruments: optical particle counter welas (PALAS, Sensor series 2300 and 2500) (Benz et al., 2005) and SIMONE (i.e., German abbreviation for Streulicht-intensitätsmessungen zum optischen Nachweis von Eispartikeln, which translates to scattering intensity measurement for the optical detection of ice) (Schnaiter et al., 2012). More details on the application of this specific combination of two instruments for the AIDA ice nucleation experiments are described in Hiranuma et al. (2014).

ACPD
14, 16493–16528, 2014

2.3 Ice nucleation parameterization and modeling

The size-independent singular ice nucleation efficiency, n_s, was calculated by normalizing the observed AIDA ice crystal concentration (N_{ice}) to the total surface area of aerosols, which can be simply calculated by multiplying the surface area of individual particle (S_i) by the total number concentration of aerosols (N_{ae}) (e.g., Niemand et al., 2012; Hoose and Möhler, 2012). For size-selected hematite particles, this linear approximation (i.e., $n_s = (-\ln(1-\alpha))/S_i \sim \alpha/S_i$) was valid independent of the ice active number fraction ($\alpha = N_{ice}/N_{ae}$). An overestimation of ice due to the use of linear approximation was only up to about a factor of three at $n_s \leq 10^{12}\,\mathrm{m}^{-2}$. Subsequently, the n_s values estimated for the wide range of experimental conditions ($-36\,^\circ\mathrm{C} < T < -78\,^\circ\mathrm{C}$ and $100\,\% < RH_{ice} <$ water saturation) were used to depict and fit constant n_s contour lines referred to here as the n_s-isolines or simply denoted as the isolines, for brevity.

The isoline-based parameterizations were derived (see Sect. 3.3) and then implemented in two atmospheric models (a single-column version of a global scale model and a convection resolving model, see Sects. 2.3.1. and 2.3.2. for model descriptions). The unique advantages of the use of both models in this study are (1) to demonstrate that our AIDA n_s-based parameterization can be directly applied in different scales of atmospheric models and (2) to estimate the number of ice crystals simulated in two different atmospheric scenarios complementally covering a wide range of atmospheric temperature and saturation conditions (ice formation at higher $RH_{ice,}$ up to $\sim 180\,\%$, and colder T, down to $\sim -70\,^\circ\mathrm{C}$). More specifically, the former represents a finely resolved parameterization-oriented model embedded in the global model, and the latter is a more physically based high-resolution grid scale model, typically used to reckon small scale complex systems for a fundamental understanding of ice formation. Altogether, results from two independent models were examined for detailed modeling of atmospheric ice formation across all scales.

We prescribed the mean size and surface area of hematite particles assuming either these particles are spherical and have a mean particle diameter of 1000 nm or the size of these particles follows a lognormal distribution, with a mean volume-equivalent diameter $\sim 1000\,\text{nm}$ ($\sigma = 0.097$), which is consistent with the AIDA experiments described earlier (Hiranuma et al., 2014). The cloud microphysical sensitivity of these two size treatments was characterized. In addition, sensitivity simulations of two lower boundaries of RH_{ice} (i.e., 100 % vs. 105 %) were also carried out. This sensitivity analysis was specifically useful to examine uncertainty involved in the TDL measurement ($RH_{ice} \pm 5\,\%$) concerning the condensed n_s spacing (up to several orders of magnitude) in a narrow RH_{ice} range at certain T region. In both models, hematite particle number concentrations are prescribed as $200\,\text{L}^{-1}$, which is about the average dust concentration simulated by the SCAM5 model over the Southern Great Plain (SGP) site in springtime. Since the n_s-isoline parameterization tested in this study is applicable at T below $-36\,^{\circ}\text{C}$, an additional parameterization was used to simulate ice formation of background particles at $T > -36\,^{\circ}\text{C}$. In specific, the aerosol-independent M92 scheme was used in this study. A combination of these parameterizations was advantageous to ensure more atmospherically relevant processes and conditions (e.g., distributions of water vapor) when compared to the application of the n_s-isoline parameterization alone.

To better understand how the AIDA n_s-based parameterization compares to other parameterizations commonly used in atmospheric models, the existing empirical parameterization of heterogeneous ice nucleation from Phillips et al. (2013, hereafter denoted as P13), was also implemented. The P13 scheme reflects the aerosol specific ice nucleation. Particularly, only the contribution by mineral dust with the background troposphere baseline surface area mixing ratio of ice-active mineral dust particles ($= 2.0 \times 10^{-6}\,\text{m}^2\,\text{kg}^{-1}$) was considered in this study. As a caveat, only ice formation occurring below water saturation is considered and, thus, Eq. (1) in Phillips et al. (2008) is used for parameterizing ice nucleation.

ACPD
14, 16493–16528, 2014

2.3.1 SCAM5

Single column models are widely used to test physical parameterizations suitable for use in the general circulation model (GCM). The model has 30 vertical levels, and model time step is set to 10 min. The single column model resembles a single column of a GCM and can be forced with either observational data or suitable model output, while the complex feedbacks between the simulated column and other columns through large-scale dynamics, except cloud detrainment from shallow and deep convection, are not considered. Therefore, it is an ideal tool for testing ice cloud parameterizations. The SCAM5 model was modified to incorporate the new parameterization developed in this study. The Barahona and Nenes (2008, 2009a, b) scheme, which provides an analytical solution of the cloud parcel model equations (hereafter BN scheme), is used for calculating the ice nucleation in cirrus clouds. The new AIDA n_s-isoline-based parameterizations as well as the P13 scheme were implemented in the model. The simulation is performed for one month (April 2010) at the United States Department of Energy's Atmospheric Radiation Measurement facility located at the SGP site (Hiranuma et al., 2014).

2.3.2 COSMO

The non-hydrostatic weather forecast model, COSMO, was also adapted to systematically investigate the impact of hematite particles in the simulated upper tropospheric conditions. More specifically, COSMO is the high resolution limited-area model, which allows an assessment of clouds and convection at a horizontal spatial resolution of 2.8 km with 50 layers of stretched vertical grids. The time step is set to 20 s. In this study, we simulated a period of two days (23 to 25 July 2011) on a domain with an extent of 450 × 450 horizontal grid points centered over the German Alps (longitude: 0.1° E to 18.7° E, latitude: 41.7° N to 53.2° N). The initial and boundary conditions were provided by the European Centre for Medium-Range Weather Forecasts, available at the Meteorological Archival and Retrieval System. Further, in order to account for

ACPD
14, 16493–16528, 2014

spatiotemporal evolution of mass and number densities of six hydrometeor classes (i.e., cloud droplets, raindrops, cloud ice, snow, graupel and hail), the two-moment bulk microphysics scheme is incorporated in our COSMO model version following the method described in Seifert and Beheng (2006) and Seifert et al. (2012). Apart from the AIDA isoline-based freezing parameterization of hematite, two other ice nucleation modes, which are specifically M92 and homogeneous nucleation of cloud or solution droplets (Kärcher et al., 2006; Ren and MacKenzie, 2005), were considered in our COSMO simulations.

3 Results

3.1 AIDA ice nucleation experiments

A series of AIDA experiments was carried out during the INUIT01 and INUIT04 campaigns to investigate the ice nucleation efficiency of well characterized hematite particles at water subsaturated conditions at $-47\,^{\circ}\mathrm{C} < T$. In the present study we also used the AIDA results reported in Skrotzki et al. (2013) and reconciled to n_s values in order to parameterize the overall ice nucleation efficiency of hematite particles up to $-78\,^{\circ}\mathrm{C}$. In total 12 expansion experiments, 4 from the INUIT campaigns and 8 from Skrotzki et al. (2013) were studied. Detailed experimental conditions and aerosol properties for these expansion experiments are summarized in Table 1. The use of different sizes of hematite particles at different temperature regions was justified by calculating the size-independent n_s values of 200 and 1000 nm diameter particles at $\sim -40\,^{\circ}\mathrm{C}$. For instance, the n_s values ($10^{10}\,\mathrm{m}^{-2}$) from these two sizes agreed very well within ±1 % $\mathrm{RH_{ice}}$ and $\pm 0.3\,^{\circ}\mathrm{C}$ of chamber conditions (i.e., INUIT04_08, 1000 nm, HALO06_19, 200 nm, and HALO06_20, 200 nm). This agreement verified the reproducibility of the AIDA chamber experiments, ice nucleation efficiency of hematite particles and size-independency in the n_s calculations. Further, an advantage of using 1000 nm diameter hematite particles was that, being of comparatively larger surface area, they were efficient in forming ice in cooling expansion experiments at $-40\,^{\circ}\mathrm{C} < T < -36\,^{\circ}\mathrm{C}$ (Hiranuma et al., 2014).

Figure 1 shows the temporal profiles of deposition nucleation experiments from HALO campaigns, including N_{ice}, gas T, $\mathrm{RH}_{\mathrm{ice}}$ and $\mathrm{RH}_{\mathrm{water}}$ measured by the TDL, and polarized light scattering properties in near-backscattering direction measured by SIMONE. The depolarization ratio, which is sensitive to ice particle nucleation and growth, can be deduced from the latter. During a typical expansion, the air mass in the vessel experiences continuous cooling (for up to 500 s) and increase in relative humidity (for up to 200 s, Fig. 1 panel i and ii). Figure 1 panel iii shows the temporal plot of the depolarization ratio. At the beginning of the expansion, the depolarization ratio increases because ice is nucleating on the hematite particles. Conversely, repartitioning of gas phase water to ice phase water due to growing ice crystals triggers the declines in both depolarization ratio (i.e., sizing effect, Schnaiter et al., 2012) and RH, usually after 100 s. The time-delay in our welas ice detection (typically 1 µm as the minimum ice detection diameter for 200 and 500 nm diameter hematite particles) due to slower depositional growth after ice nucleation at colder T is accounted in our error analyses (Fig. 2). We note that we evaluated only up to several hundred seconds of each expansion experiment as the ice nucleating period. Similar experimental profiles for INUIT campaigns are presented in Supplement Fig. S1.

Figure 2 illustrates the initial n_{s}-isoline curves in the T-$\mathrm{RH}_{\mathrm{ice}}$ space. Constant n_{s}-isoline curves are obtained by fitting second degree polynomial fit equations to the constant n_{s} magnitudes calculated at various T and $\mathrm{RH}_{\mathrm{ice}}$ (see Supplement for more details). Previous AIDA measurements of immersion freezing (i.e., INUIT04_13 and INUIT01_28 from Hiranuma et al., 2014) are also shown and used to constrain the fitted curves. Figure 2 shows several important features of n_{s}-isoline curves. First, below $-60\,^{\circ}\mathrm{C}$, n_{s}-isolines showed an increase in $\mathrm{RH}_{\mathrm{ice}}$ required to maintain constant n_{s} (i.e., $n_{\mathrm{s}} > 2.5 \times 10^{8}\,\mathrm{m}^{-2}$) with decreasing T. For example, at a $\mathrm{RH}_{\mathrm{ice}} = 120\,\%$ and $T = -75\,^{\circ}\mathrm{C}$ conditions, cooling by $1\,^{\circ}\mathrm{C}$ corresponds to a 10 % decrease in n_{s}. This observation is interesting because the increase in $\mathrm{RH}_{\mathrm{ice}}$ required to maintain constant

ACPD
14, 16493–16528, 2014

n_s values is consistent with the CNT for deposition nucleation (Eq. A11 in Hoose and Möhler, 2012). Second, the highest sensitivity of RH_{ice} is observed in a region where n_s-isolines are perpendicular to temperature-isolines ($\sim -60\,^{\circ}C < T <\sim -50\,^{\circ}C$). Here, n_s is almost independent of T, and dependent on only RH_{ice}. Finally, we observed strong T-dependent nucleation near water saturation (i.e., while cooling along the water saturation line toward $\sim -50\,^{\circ}C$). For example, at constant RH_{ice} (e.g., 114 %), cooling for 1 °C from −41 to −42 °C corresponds to an increase in n_s of approximately a half order of magnitude (see inset of Fig. 2), suggesting n_s values depend on temperature. Interestingly, we observed a continuous increase in n_s while concurrent cooling even after depletion of supersaturation below −40 °C (Supplement Fig. S2). CNT does not explain this predominant T contribution near water saturation (Fig. A1 in Hoose and Möhler, 2012). Therefore, other microphysical processes at the particle surface and/or perhaps even within the bulk phase may be responsible for this T-dependent behavior and pointed to a new freezing process in this study. In particular, we suspect that water condensation on the particle surface plays an important role on subsequent freezing. Supportively, the surfaces of our hematite particles are not perfectly smooth and contain some active sites (e.g., pores and steps, Hiranuma et al., 2014). Moreover, water vapor may preferentially fill the surface cavities due to the reduced saturation pressure in pores or at steps because of negative curvature Kelvin effects (Marcolli, 2014), thus leading to namely "surface condensation freezing (SCF)". As described in previously published literatures (Christenson, 2013; Marcolli, 2014), SCF may have plausible relevance to homogeneous nucleation (i.e., spontaneous ice nucleation in supercooled aerosol) at relevant T ($< -36\,^{\circ}C$) and/or immersion mode freezing in water subsaturated conditions. Thus, SCF may arise from both homogeneous and heterogeneous nucleation.

3.2 Comparison with previous studies

We now compare the n_s-isolines of hematite particles to previous measurements that were derived using different aerosol species. This comparison is performed to (1) confirm our n_s fit reproduces the overall trend shown by previous studies, which were conducted within certain T-RH_{ice} conditions, and (2) demonstrate that the parameterization with laboratory-synthesized hematite particles quantitatively represents ice nucleation properties of atmospheric dust particles. We note that hematite is an example of atmospheric mineral dust particles that consists of metallic component (Mishra et al., 2012), which can be also found as cloud-borne particles (Matsuki et al., 2010). Natural hematite oftentimes exists in the supermicron sized silt particles and accounts for a few percent of the total dust particle mass (Claquin et al., 1999).

In Fig. 3, our n_s-isolines of hematite particles were compared to previous deposition freezing observations on natural Saharan desert dust (SD2, Möhler et al., 2006), reference Arizona test dust (ATD, Möhler et al., 2006; Welti et al., 2009), volcanic ash (Steinke et al., 2011), soot (Möhler et al., 2005), clay minerals (Welti et al., 2009; Koehler et al., 2010) and organics (Shilling et al., 2006; Wang and Knopf, 2011). Reported previous experimental studies used various types of ice nucleation instruments, such as substrate supported cold stages coupled with an optical microscope (Shilling et al., 2006; Wang and Knopf, 2011), mobile ice nuclei counters (Koehler et al., 2010; Welti et al., 2009) and the AIDA cloud simulation chamber (Möhler et al., 2005, 2006; Steinke et al., 2011), and revealed the importance of both RH_{ice} and temperature on deposition mode ice nucleation of specific particle compositions. In Fig. 3 panel A, we present previous AIDA results for dusts, ash and soot. Specifically, we utilized the T-RH_{ice} data at $\alpha = 0.08$ of SD2 and ATD reported in previous AIDA study (Möhler et al., 2006) in order to define isolines. We note that an α of 0.08 corresponds to $\sim 10^{11}\,\mathrm{m}^{-2}$ in n_s assuming uniform distributions of spherical particles that have 0.5 µm diameter ($n_s = (-\ln(1-\alpha))/(\pi(0.5\times10^{-6})^2)$), which is fairly in a good agreement with the $10^{11}\,\mathrm{m}^{-2}$ n_s-isoline of hematite particles. For volcanic ash, we adapted n_s values (10^9, 5×10^9 and $10^{10}\,\mathrm{m}^{-2}$) that were originally reported in Steinke et al. (2011). Möhler et al. (2005) identified the ice nucleation onset of soot at the initial increase in polarized light scattering intensity in near-backscattering direction at 488 nm (n_s values are inaccessible). Except these AIDA studies, other isolines in Fig. 3b and c were defined based on

ACPD
14, 16493–16528, 2014

Title Page
Abstract | Introduction
Conclusions | References
Tables | Figures
◀| |▶
◀ ▶
Back | Close
Full Screen / Esc
Printer-friendly Version
Interactive Discussion

the reported ice nucleation measurements. For instance, Koehler et al. (2010) studied the deposition mode nucleation of size-selected (i.e., 200 nm, 300 nm, 400 nm) natural dusts, and reported ice nucleation conditions (T and RH_{ice}) of ATD at $\alpha = 0.01$ and of Canary Island Dust and SD2 at $\alpha = 0.05$. Welti et al. (2009) also studied the deposition nucleation abilities of size-segregated mineral dusts (i.e., 100 to 800 nm diameter of ATD, illite, kaolinite and montmorillonite) based on $\alpha = 0.01$. Shilling et al. (2006) reported the ice nucleation onsets of ammonium sulfate and maleic acid detected by the decreasing partial pressure of water with FTIR-reflection absorption spectroscopy (e.g., 1 in 10^5 nucleation at about $-33\,^{\circ}$C for spherical particle size 1 to 10 µm diameter). Wang and Knopf. (2011) investigated the deposition freezing of various mineral and organic particles including kaolinite, Suwannee River standard fulvic acid and Leonardite standard humic acid particles. The authors reported the mean size of particles and associated ice activated fractions at given T-RH_{ice}.

As seen in Fig. 3, the results from previous studies suggest the necessity of increasing RH_{ice} to maintain constant n_s below $T \sim -55\,^{\circ}$C and also imply nucleation triggered by SCF in the region where data and isolines approach water saturation where temperature plays a significant role on ice nucleation. It can also be observed that the contour of our new n_s-isoline parameterization of cubic hematite particles in T-RH_{ice} coordinates generally agrees with the onsets from previous studies of other atmospherically relevant aerosols. In particular, the n_s-isolines estimated from ATD and SD2 ($\sim 10^{11}$ m^{-2}, Fig. 3a), which reasonably agree with hematite n_s-isoline, suggest that atmospheric dust may have similar deposition mode ice nucleation efficiency.

3.3 n_s-Isoline-based Parameterizations

Next, we parameterized the ice nucleation efficiency of hematite particles over a wide range of T-RH_{ice}. Three types of parametrical descriptions used in this study are shown in Fig. 4. First, based on the AIDA experimental results, a series of the constant n_s curves was interpolated to produce isolines in the range of 10^6 m^{-2} $< n_s < 10^{12}$ m^{-2}

(Fig. 4a). The lower bound of n_s value ($10^6\,m^{-2}$) was set based on the minimum n_s observed during AIDA expansions. The method used to constrain the n_s-isolines above 100 % RH_{ice} as discussed in the Supplement (Fig. S3). Above the upper bound of $10^{12}\,m^{-2}$, n_s presumably remains constant up to the water saturation line in T-RH_{ice} space. This assumption is valid in the present study because this n_s upper limit was hardly reached in our modeling case. However, we note that more cloud simulation chamber measurements and data points for $n_s >> 10^{12}\,m^{-2}$ are necessary in order to correctly constrain the n_s upper limit. It is also noteworthy that the modeled ice crystal number concentration (L^{-1}) derived from ice nucleation of hematite in this study is approximated by multiplying n_s by a simulated total surface of hematite ($6.3 \times 10^{-10}\,m^2\,L^{-1}$).

In the second fit approach (Fig. 4b), the interpolated n_s values were used to formulate n_s-isoline with a third degree-polynomial fit as a function of T (°C) and RH_{ice} (%) as

$$\begin{aligned} n_s^{3d}(T,\mathrm{RH_{ice}}) = & -3.777\times10^{13} - 7.818\times10^{11}\cdot T + 4.252\times10^{11}\cdot \mathrm{RH_{ice}} \\ & - 4.598\times10^{9}\cdot T^2 + 6.952\times10^{9}\cdot T\cdot \mathrm{RH_{ice}} - 1.111\times10^{9}\cdot \mathrm{RH_{ice}^2} \\ & - 2.966\times10^{6}\cdot T^3 + 2.135\times10^{7}\cdot T^2\cdot \mathrm{RH_{ice}} - 1.729\times10^{7}\cdot T\cdot \mathrm{RH_{ice}^2} \\ & - 9.438\times10^{5}\cdot \mathrm{RH_{ice}^3} \\ & \text{for } -78\,^\circ\mathrm{C} < T < -36\,^\circ\mathrm{C} \text{ and } 100\,\% < \mathrm{RH_{ice}} < \text{water saturation} \end{aligned} \tag{1}$$

where $n_s^{3d}(T,RH_{ice})$ is the n_s derived from third degree fit. The resulting spatial plot of isolines for constant n_s is shown in Fig. 4b. The third approach (Fig. 4c) was to apply the equivalent n_s for deposition nucleation of hematite particles parameterized by following the method introduced in Phillips et al. (2008 and 2013). More specifically, we took an approach to characterize the nucleation activity solely of mineral dust through the deposition mode by adapting the Eq. (1) from Phillips et al. (2008), which accounts for nucleation under water subsaturated conditions, and excluded contribution at water saturation i.e., Eq. (2) from Phillips et al. (2008). Note that the upper boundary of temperature −36 °C was assigned as the interface between immersion mode- and deposition mode ice nucleation (Hiranuma et al., 2014), and the lower boundary of −78 °C is the limit introduced by interpolating the hematite-isoline curves. To conclude, the discrepancy between a new parameterization and P13 is substantially large, and the consequence of this discrepancy towards cloud properties is demonstrated in the following section.

3.4 Model simulations

Figure 5 shows the SCAM5 results for monthly mean profiles of the simulated ice crystal number concentrations over the ARM SGP site for five cases. These include the pure homogeneous ice nucleation case (Simulation A), three cases with contributions from both the homogeneous and heterogeneous ice nucleation (hereafter combined case) described in Fig. 4 (Simulations B, C and D) and the simulation of the different lower boundaries of RH_{ice} (RH_i^*, Simulation D). We observe that ice crystal formation from heterogeneous ice nucleation processes inhibits homogenous ice nucleation and reduces the ice number concentrations significantly for the AIDA parameterizations (Fig. 4a and b). In contrast, due to the much smaller ice crystal production from P13, as indicated in the pure heterogeneous case shown in Fig. 5, homogeneous ice nucleation in the P13 case (Fig. 4c) is less affected by heterogeneous nucleation. The differences between the four parameterizations used in this study are small for both the combined cases and the pure heterogeneous cases. This is because the BN scheme used in SCAM5 is based on parcel model theory and uses the predicted maximum ice supersaturation (S_{max}) to calculate deposition ice nucleation rates. S_{max} is determined by assuming that the supersaturation will reach its maximum where the depletion of water vapor balances the supersaturation increase from cooling in a cloud parcel (i.e., BN scheme). The three parameterizations have largest differences when RH_{ice} is below 120 %, while S_{max} calculated in the model is often larger than 115 %. This also explains the low sensitivity of N_{ice} to the lower bound of the onset RH_{ice} value (Figs. 5 and 6). We further investigate the impact of assuming different particle size distributions in the

ACPD
14, 16493–16528, 2014

calculation (not shown). The impact is small and negligible. The negligible sensitivity to the choice of AIDA parameterizations in SCAM5 simulations (Simulation A and B of Figs. 5 and 6) as well as the negligible sensitivity to the lower bound of RH_{ice} value for ice nucleation, RHi^* in Figs. 5 and 6, reflects the limitation of SCAM5 as a large-scale model, which can not explicitly resolve the sub-grid (for GCM grid-box) variability of the supersaturation.

Figure 7 summarizes results of the COSMO model for the vertical profiles of N_{ice} simulated using the three different parameterization schemes (corresponding to Fig. 4a–c) in combination with homogeneous freezing. N_{ice} was spatially averaged over all cloudy areas of the model domain for freezing conditions of cubic hematite particles. As shown in Fig. 7, the mean N_{ice} resulting from the parameterization based on P13 is smaller than that from the AIDA n_s-isoline-based parameterization by more than two orders of magnitude. Unlike the SCAM5 results, the COSMO results show the sensitivity to the different lower boundaries of RH_{ice} (i.e., $RHi^* = 105\,\%$, Simulation D). For instance, the mean N_{ice} below $-36\,^{\circ}C$ with a higher RH_{ice} boundary (105 %) is reduced by 12 %. This difference is perhaps due to the use of finely resolved grid-scale humidity in COSMO rather than parameterizing S_{max} as done in SCAM5 (Gettelman et al., 2010). Figure 8 illustrates the differences between P13 and the AIDA results depending on T and RH_{ice}. Simulated N_{ice} are segregated in fine T and RH_{ice} spacing (1 K and 2 % bins, respectively) based on the thermodynamic conditions under which ice crystals were formed in COSMO and summed up over the time of simulation. This enables us to estimate the relative contribution of different thermodynamic conditions to the simulated ice formation. Our result shows less ice crystal formation with P13 compared to the AIDA n_s-isoline-based parameterization. The observed discrepancy between the new parameterization and P13 may largely reflect the difference in parameterization based on lab- or field data. Furthermore, strong supersaturation dependence of n_s at cold T was not well constrained by P13, presumably due to a limited amount of data.

ACPD
14, 16493–16528, 2014

4 Discussions

As described in previous section, the deposition mode freezing cannot solely explain the n_s-isoline observation below water saturation ($-50\,^\circ\mathrm{C} < T < -36\,^\circ\mathrm{C}$ in Fig. 2), and we presumed that SCF may play an important role in this region. Nevertheless, further insight and evidence of SCF beyond cloud simulation chamber observations to correctly understand the contributions of both homogeneous and heterogeneous nucleation are needed. High resolution microscopic techniques with an integrated continuous cooling setup are needed to visualize the freezing process of a single-particle and to fully understand the complex freezing processes involved in SCF upon particle surfaces, thereby solidifying our premise.

A comparison of the new parameterization to a previous empirical parameterization (P13) showed that the new AIDA n_s-isoline-based scheme predicts more ice (Figs. 4–8). In particular, T-$\mathrm{RH}_{\mathrm{ice}}$ dependence of N_{ice} and n_s at cold T that may coincide in the upper troposphere and deserves more attention. Substantial differences between the empirical approach of P13 and our parameterization developed in this study are presumably attributed to the difference in lab- or field data, highlighting the need for further characterizations of atmospherically relevant substrates and their ice nucleation activities in laboratory settings. Nevertheless, Niemand et al. (2012) demonstrated that different dusts exhibit similar n_s in immersion mode freezing and perhaps such a similarity remains true for deposition mode ice nucleation. In fact, comparison between our AIDA n_s-based parameterization with hematite particles and Möhler et al. (2006) with ATD and SD2 (Fig. 3a) provides indication on the validity of the assumption to treat all dust as hematite in deposition mode.

Finally, in order to further develop more atmospherically relevant parameterizations beyond fit-based parameterizations with artificial test aerosol, one may explore (extend our n_s-isoline study) to identify the relationship between $1/T$ and $\ln S_{\mathrm{ice}}$ for constant nucleation rate or n_s based on the CNT (i.e., Eqs. A10 and A11 in Hoose and Möhler, 2012). In this way, the composition specific n_s (T-S_{ice}) values, where the transition from

Discussion Paper | Discussion Paper | Discussion Paper | Discussion Paper |
ACPD
14, 16493–16528, 2014
A comprehensive parameterization of heterogeneous ice nucleation of dust
N. Hiranuma et al.

SCF to deposition nucleation (or visa-versa) occurs, may be better constrained and can be further used as an computationally inexpensive parameterization for a model.

5 Conclusion

In this work, a new heterogeneous ice nucleation parameterization was developed using results obtained from AIDA cloud simulation chamber experiments. The new n_s-isoline-based parameterization is applicable to a wide temperature range from −36 to −78 °C and thereby allows the examination of ice nucleation spectra in a simple framework for modeling application.

Our experimental results provide a good basis for the T and RH_{ice} dependency of deposition nucleation, and the formulated hematite n_s-isolines are comparable to that of desert dust samples. Therefore, our results with synthesized hematite particles can also be relevant for cirrus applications despite of less atmospheric relevancy when compared to natural hematite. Our isoline formulation also suggested three different ice nucleation pathways over the wide range of temperature. In specific, a RH_{ice}-dependent ice nucleation regime was observed at temperature below ~ -60 °C, where deposition mode was presumably responsible to trigger ice nucleation. At $-60\,^{\circ}C < T < -50\,^{\circ}C$, ice nucleation efficiency was T-independent (i.e., RH_{ice}-dependent). Conversely, the predominance of T on ice nucleation was observed near the water saturation condition ($T >\sim -50$ °C), which may be indicative of nucleation due to condensation of water at the particle surface followed by homogeneous freezing of the condensed water (i.e., SCF). Elaborating observed suppression of SCF near water saturation and enlightening the physical processes on observed transitions in nucleation modes for various types of atmospheric particles are important as future works.

Our conceptual model examinations also considered the competition between heterogeneous freezing and homogeneous freezing of solution particles to evaluate the relative importance of the different freezing processes in two models (SCAM5 and COSMO). The inhibition of homogeneous nucleation due to heterogeneous freezing was commonly observed in both SCAM5 and COSMO simulations. The minimum deviation in estimated N_{ice} from the choices of the minimum RH_{ice} value for ice formation (100 or 105 %) with our new parameterization was observed for SCAM5 when compared to COSMO, suggesting different model sensitivity to the lower bound of the RH_{ice} value caused by the presence of the model resolved supersaturation to calculate the ice nucleation rate. Overall, our new hematite-based parameterization strongly suggests the role of T and suppression in ice nucleation when compared to the existing empirical parameterization, presumably allowing more ice activation under water subsaturated conditions.

Author Contribution

N. Hiranuma and O. Möhler designed and conceived the experiments. Parameterizations were implemented by N. Hiranuma, I. Steinke and M. Paukert. M. Paukert, and K. Zhang carried out modeling studies with input from C. Hoose, N. Hiranuma and G. Kulkarni. M. Schnaiter analyzed SIMONE data. H. Saathiff contributed to TDL measurements and analysis. The manuscript was written by N. Hiranuma. All authors discussed the results and contributed ideas to the manuscript.

The Supplement related to this article is available online at doi:10.5194/acpd-14-16493-2014-supplement.

Acknowledgements. This work was supported by German Research Society (DfG) under contracts MO668/4-1 and HO4612/1-1 within FOR 1525 INUIT and the Helmholtz Association through the research programme "Atmosphere and Climate (ATMO)". The authors acknowledge partial financial support by Deutsche Forschungsgemeinschaft and Open Access Publishing Fund of Karlsruhe Institute of Technology. K. Zhang and G. Kulkarni acknowledge support from the Department of Energy (DOE) Atmospheric System Research Program and thank J. Fast for useful discussions. The Pacific Northwest National Laboratory is operated for DOE by Battelle Memorial Institute under contract DE-AC05-76RLO 1830. We would like to thank R. Buschbacher, T. Chudy, E. Kranz, G. Scheurig and S. Vogt for their professional support for the AIDA chamber operation during the INUIT campaigns. We also thank P. Weidler and S. Jaeger for support in preparing the hematite particles. Contribution from M. Hummel on the model setup is gratefully acknowledged.

The service charges for this open access publication have been covered by a Research Centre of the Helmholtz Association.

References

Baldauf, M., Seifert, A., Förstner, J., Majewski, D., Raschendorfer, M., and Reinhardt, T.: Operational convective-scale numerical weather prediction with the COSMO model: description and sensitivities, Mon. Weather Rev., 139, 3887–3905, doi:10.1175/MWR-D-10-05013.1, 2011.

Barahona, D. and Nenes, A.: Parameterization of cirrus cloud formation in large-scale models: homogeneous nucleation, J. Geophys. Res., 113, D11211, doi:10.1029/2007JD009355, 2008.

Barahona, D. and Nenes, A.: Parameterizing the competition between homogeneous and heterogeneous freezing in cirrus cloud formation – monodisperse ice nuclei, Atmos. Chem. Phys., 9, 369–381, doi:10.5194/acp-9-369-2009, 2009a.

Barahona, D. and Nenes, A.: Parameterizing the competition between homogeneous and heterogeneous freezing in ice cloud formation – polydisperse ice nuclei, Atmos. Chem. Phys., 9, 5933–5948, doi:10.5194/acp-9-5933-2009, 2009b.

Barahona, D., Rodriguez, J., and Nenes, A.: Sensitivity of the global distribution of cirrus ice crystal concentration to heterogeneous freezing, J. Geophys. Res., 115, D23213, doi:10.1029/2010JD014273, 2010.

Benz, S., Megahed, K., Möhler, O., Saathoff, H., Wagner, R., and Schurath, U.: T-dependent rate measurements of homogeneous ice nucleation in cloud droplets using a large atmospheric simulation chamber, J. Photoch. Photobio. A, 176, 208–217, 2005.

ACPD
14, 16493–16528, 2014

Boucher, O., Randall, D., Artaxo, P., Bretherton, C., Feingold, G., Forster, P., Kerminen, V.-M., Kondo, Y., Liao, H., Lohmann, U., Rasch, P., Satheesh, S. K., Sherwood, S., Stevens, B., and Zhang, X. Y.: Clouds and aerosols, in: Climate Change 2013: The Physical Science Basis. Contribution of Working Group I to the Fifth Assessment Report of the Intergovernmental Panel on Climate Change, edited by: Stocker, T. F., Qin, D., Plattner, G.-K., Tignor, M., Allen, S. K., Boschung, J., Nauels, A., Xia, Y., Bex, V., and Midgley, P. M., Cambridge University Press, Cambridge, United Kingdom and New York, NY, USA, 2013.

Christenson, H.: Two-step crystal nucleation via capillary condensation, Cryst. Eng. Comm., 15, 2030–2039, 2013.

Claquin, T., Schulz, M., and Balkanski, Y.: Modeling the mineralogy of atmospheric dust sources, J. Geophys. Res., 104, 22243–22256, 1999.

Connolly, P. J., Möhler, O., Field, P. R., Saathoff, H., Burgess, R., Choularton, T., and Gallagher, M.: Studies of heterogeneous freezing by three different desert dust samples, Atmos. Chem. Phys., 9, 2805–2824, doi:10.5194/acp-9-2805-2009, 2009.

Cziczo, D. J., Froyd, K. D., Hoose, C., Jensen, E. J., Diao, M., Zondlo, M. A., Smith, J. B., Twohy, C. H., and Murphy, D. M.: Clarifying the dominant sources and mechanisms of cirrus cloud formation, Science, 340, 1320–1324, 2013.

DeMott, P., Möhler, O., Stetzer, O., Vali, G., Levin, Z., Petters, M. D., Murakami, M., Leisner, T., Bundke, U., Klein, H., Kanji, Z. A., Cotton, R., Jones, H., Benz, S., Brinkmann, M., Rzesanke, D., Saathoff, H., Nicolet, M., Saito, A., Nillius, B., Bingemer, H., Abbatt, J., Ardon, K., Ganor, E., Georgakopoulos, D. G., and Saunders, C.: Resurgence in ice nuclei measurement research, B. Am. Meterol. Soc., 92, 1623–1625, 2011.

Doms, G., Förster, J., Heise, E., Herzog, H.-J., Mironov, D., Raschendorfer, M., Reinhardt, T., Ritter, B., Schrodin, R., Schulz, J.-P., and Vogel, G.: A description of the nonhydrostatic regional COSMO Model, Part II: Physical parameterization, Technical Report, Deutscher Wetterdienst, 154 pp., 2011.

Fahey, D. W., Gao, R.-S., Möhler, O., Saathoff, H., Schiller, C., Ebert, V., Krämer, M., Peter, T., Amarouche, N., Avallone, L. M., Bauer, R., Bozóki, Z., Christensen, L. E., Davis, S. M., Durry, G., Dyroff, C., Herman, R. L., Hunsmann, S., Khaykin, S. M., Mackrodt, P., Meyer, J., Smith, J. B., Spelten, N., Troy, R. F., Vömel, H., Wagner, S., and Wienhold, F. G.: The AquaVIT-1 intercomparison of atmospheric water vapor measurement techniques, Atmos. Meas. Tech. Discuss., 7, 3159–3251, doi:10.5194/amtd-7-3159-2014, 2014.

Gettelman, A., Hegglin, M. I., Son, S.-W., Kim, J., Fujiwara, M., Birner, T., Kremser, S., Rex, M., Añel, J. A., Akiyoshi, H., Austin, J., Bekki, S., Braesike, P., Brühl, C., Butchart, N., Chipperfield, M., Dameris, M., Dhomse, S., Garny, H., Hardiman, S. C., Jöckel, P., Kinnison, D. E., Lamarque, J. F., Mancini, E., Marchand, M., Michou, M., Morgenstern, O., Pawson, S., Pitari, G., Plummer, D., Pyle, J. A., Rozanov, E., Scinocca, J., Shepherd, T. G., Shibata, K., Smale, D., Teyssèdre, H., and Tian, W.: Multimodel assessment of the upper troposphere and lower stratosphere: tropics and global trends, J. Geophys. Res., 115, D00M08, doi:10.1029/2009JD013638, 2010.

Hiranuma, N., Hoffmann, N., Kiselev, A., Dreyer, A., Zhang, K., Kulkarni, G., Koop, T., and Möhler, O.: Influence of surface morphology on the immersion mode ice nucleation efficiency of hematite particles, Atmos. Chem. Phys., 14, 2315–2324, doi:10.5194/acp-14-2315-2014, 2014.

Hoose, C. and Möhler, O.: Heterogeneous ice nucleation on atmospheric aerosols: a review of results from laboratory experiments, Atmos. Chem. Phys., 12, 9817–9854, doi:10.5194/acp-12-9817-2012, 2012.

Hoose, C., Kristjánsson, J. E., Chen, J.-P., and Hazra, A.: A classical-theory-based parameterization of heterogeneous ice nucleation by mineral dust, soot and biological particles in a global climate model, J. Atmos. Sci., 67 2483–2503, 2010.

Kärcher, B. and Lohmann, U.: A parameterization of cirrus cloud formation: heterogeneous freezing, J. Geophys. Res., 108, 4402, doi:10.1029/2002JD003220, 2003.

Kärcher, B., Hendricks, J., and Lohmann, U.: Physically based parameterization of cirrus cloud formation for use in global atmospheric models, J. Geophys. Res., 111, D01205, doi:10.1029/2005JD006219, 2006.

Khvorostyanov, V. I. and Curry, J. A.: The theory of ice nucleation by heterogeneous freezing of deliquescent mixed CC N. Part I: Critical radius, energy, and nucleation rate, J. Atmos. Sci., 61, 2676–2691, 2004.

Koehler, K. A., Kreidenweis, S. M., DeMott, P. J., Petters, M. D., Prenni, A. J., and Möhler, O.: Laboratory investigations of the impact of mineral dust aerosol on cold cloud formation, Atmos. Chem. Phys., 10, 11955–11968, doi:10.5194/acp-10-11955-2010, 2010.

Koop, T., Luo, B., Tsias, A., and Peter, T.: Water activity as the determinant for homogeneous ice nucleation in aqueous solutions, Nature, 406, 611–614, 2000.

Liu, X. and Penner, J. E.: Ice nucleation parameterization for global models, Meteorol. Z., 14, 499–514, 2005.

Liu, X., Shi, X., Zhang, K., Jensen, E. J., Gettelman, A., Barahona, D., Nenes, A., and Lawson, P.: Sensitivity studies of dust ice nuclei effect on cirrus clouds with the Community Atmosphere Model CAM5, Atmos. Chem. Phys., 12, 12061–12079, doi:10.5194/acp-12-12061-2012, 2012.

Marcolli, C.: Deposition nucleation viewed as homogeneous or immersion freezing in pores and cavities, Atmos. Chem. Phys., 14, 2071–2104, doi:10.5194/acp-14-2071-2014, 2014.

Matsuki, A., Schwarzenboeck, A., Venzac, H., Laj, P., Crumeyrolle, S., and Gomes, L.: Cloud processing of mineral dust: direct comparison of cloud residual and clear sky particles during AMMA aircraft campaign in summer 2006, Atmos. Chem. Phys., 10, 1057–1069, doi:10.5194/acp-10-1057-2010, 2010.

Meyers, M. P., DeMott, P. J., and Cotton, W. R.: New primary ice nucleation parameterizations in an explicit cloud model, J. Appl. Meteorol., 31, 708–721, 1992.

Mishra, S. K., Tripathi, S. N., Aggarwal, S. G., and Arola, A.: Optical properties of accumulation mode, polluted mineral dust: effects of particle shape, hematite content and semi-external mixing with carbonaceous species, Tellus B, 64, 18536, doi:10.3402/tellusb.v64i0.18536, 2012.

Möhler, O., Stetzer, O., Schaefers, S., Linke, C., Schnaiter, M., Tiede, R., Saathoff, H., Krämer, M., Mangold, A., Budz, P., Zink, P., Schreiner, J., Mauersberger, K., Haag, W., Kärcher, B., and Schurath, U.: Experimental investigation of homogeneous freezing of sulphuric acid particles in the aerosol chamber AIDA, Atmos. Chem. Phys., 3, 211–223, doi:10.5194/acp-3-211-2003, 2003.

Möhler, O., Linke, C., Saathoff, H., Schnaiter, M., Wagner, R., Mangold, A., Krämer, M., and Schurath, U.: Ice nucleation on flame soot aerosol of different organic carbon content, Meteorol. Z., 14, 477–484, 2005.

Möhler, O., Field, P. R., Connolly, P., Benz, S., Saathoff, H., Schnaiter, M., Wagner, R., Cotton, R., Krämer, M., Mangold, A., and Heymsfield, A. J.: Efficiency of the deposition mode ice nucleation on mineral dust particles, Atmos. Chem. Phys., 6, 3007–3021, doi:10.5194/acp-6-3007-2006, 2006.

Murray, B. J., O'Sullivan, D., Atkinson, J. D., and Webb, M. E.: Ice nucleation by particles immersed in supercooled cloud droplets, Chem. Soc. Rev., 41, 6519–6554, 2012.

Neale, R. B., Chen, C.-C., Gettelman, A., Lauritzen, P. H., Park, S., Williamson, D. L., Conley, A. J., Garcia, R., Kinnison, D., Lamarque, J.-F., Marsh, D., Mills, M., Smith, A. K., Tilmes, S., Vitt, F., Morrison, H., Cameron-Smith, P., Collins, W. D., Iacono, M. J., Easter, R. C., Ghan, S. J., Liu, X., Rasch, P. J., and Taylor, M. A.: Description of the NCAR Community Atmosphere Model (CAM5.0), Tech. Rep. NCAR/TN-486-STR, NCAR, available at: http://www.cesm.ucar.edu/models/cesm1.0/cam/ (last access: 8 January 2013), 2010.

Niemand, M., Möhler, O., Vogel, B., Vogel, H., Hoose, C., Connolly, P., Klein, H., Bingemer, H., DeMott, P., Skrotzki, J., and Leisner, T.: A particle-surface-area-based parameterization of immersion freezing on mineral dust particles, J. Atmos. Sci., 69, 3077–3092, 2012.

Phillips, V. T. J., DeMott, P. J., and Andronache, C.: An empirical parameterization of heterogeneous ice nucleation for multiple chemical species of aerosol, J. Atmos. Sci., 65, 2757–2783, 2008.

Phillips, V. T. J., DeMott, P. J., Andronache, C., Pratt, K. A., Prather, K. A., Subramanian, R., and Twohy, C.: Improvements to an empirical parameterization of heterogeneous ice nucleation and its comparison with observations, J. Atmos. Sci., 70, 378–409, doi:10.1175/JAS-D-12-080.1, 2013.

Pruppacher, H. R. and Klett, J. D.: Microphysics of Clouds and Precipitation, Atmospheric and Oceanographic Sciences Library, Kluwer Academic Publishers, Dordrecht, the Netherlands, 309–360, 1997.

Ren, C. and Mackenzie, A. R.: Cirrus parameterization and the role of ice nuclei, Q. J. Roy. Meteor. Soc., 131, 1585–1605, 2005.

Sakai, T., Orikasa, N., Nagai, T., Murakami, M., Tajiri, T., Saito, A., Yamashita, K., and Hashimoto, A.: Balloon-borne and Raman lidar observations of Asian dust and cirrus cloud properties over Tsukuba, Japan, J. Geophys. Res., 119, 3295–3308, doi:10.1002/2013JD020987, 2014.

Sassen, K. and Khvorostyanov, V. I.: Cloud effects from boreal forest fire smoke: evidence for ice nucleation from polarization lidar data and cloud model simulations, Environ. Res. Lett., 3, 025006, doi:10.1088/1748-9326/3/2/025006, 2008.

Schnaiter, M., Büttner, S., Möhler, O., Skrotzki, J., Vragel, M., and Wagner, R.: Influence of particle size and shape on the backscattering linear depolarisation ratio of small ice crystals – cloud chamber measurements in the context of contrail and cirrus microphysics, Atmos. Chem. Phys., 12, 10465–10484, doi:10.5194/acp-12-10465-2012, 2012.

Seifert, A. and Beheng, K. D.: A two-moment cloud microphysics parameterization for mixed-phase clouds, Part I: Model description, Meteorol. Atmos. Phys., 92, 45–66, 2006.

ACPD
14, 16493–16528, 2014

A comprehensive parameterization of heterogeneous ice nucleation of dust

N. Hiranuma et al.

Seifert, A., Köhler, C., and Beheng, K. D.: Aerosol-cloud-precipitation effects over Germany as simulated by a convective-scale numerical weather prediction model, Atmos. Chem. Phys., 12, 709–725, doi:10.5194/acp-12-709-2012, 2012.

Shilling, J. E., Fortin, T. J., and Tolbert, M. A.: Depositional ice nucleation on crystalline organic and inorganic solids, J. Geophys. Res., 111, D05207, doi:10.1029/2005JD006664, 2006.

Skrotzki, J., Connolly, P., Schnaiter, M., Saathoff, H., Möhler, O., Wagner, R., Niemand, M., Ebert, V., and Leisner, T.: The accommodation coefficient of water molecules on ice – cirrus cloud studies at the AIDA simulation chamber, Atmos. Chem. Phys., 13, 4451–4466, doi:10.5194/acp-13-4451-2013, 2013.

Steinke, I., Möhler, O., Kiselev, A., Niemand, M., Saathoff, H., Schnaiter, M., Skrotzki, J., Hoose, C., and Leisner, T.: Ice nucleation properties of fine ash particles from the Eyjafjallajökull eruption in April 2010, Atmos. Chem. Phys., 11, 12945–12958, doi:10.5194/acp-11-12945-2011, 2011.

Storelvmo, T. and Herger, N.: Cirrus cloud susceptibility to the injection of ice nuclei in the upper troposphere, J. Geophys. Res., 119, 2375–2389, doi:10.1002/2013JD020816, 2014.

Sugimoto, T. and Sakata, K.: Preparation of monodisperse pseudocubic α-Fe_2O_3 particles from condensed ferric hydroxide gel, J. Colloid Interface Sci., 152, 2, 587–590, 1992.

Vali, G.: Nucleation terminology, J. Aerosol Sci., 16, 575–576, 1985.

Vragel, M.: Messung klimarelevanter optischer Eigenschaften von Mineralstaub im Labor, Faculty of Physics, Karlsruhe Institute of Technology, Karlsruhe, 162 pp., 2009.

Wang, B. and Knopf, D.: Heterogeneous ice nucleation on particles composed of humic-like substances impacted by O_3, J. Geophys. Res., 116, D03205, doi:10.1029/2010JD014964, 2011.

Welti, A., Lüönd, F., Stetzer, O., and Lohmann, U.: Influence of particle size on the ice nucleating ability of mineral dusts, Atmos. Chem. Phys., 9, 6705–6715, doi:10.5194/acp-9-6705-2009, 2009.

Welti, A., Kanji, Z. A., Lüönd, F., Stetzer, O., and Lohmann, U.: Exploring the mechanisms of ice nucleation on kaolinite: from deposition nucleation to condensation freezing, J. Atmos. Sci., 71, 16–36, doi:10.1175/JAS-D-12-0252.1, 2014.

ACPD
14, 16493–16528, 2014

Table 1. Summary of aerosol measurements and AIDA ice nucleation experiments.

	Aerosol Measurements			Ice Nucleation Measurements				
Experiment ID	Hematite Diameter, nm	Total Number Conc., cm^{-3}	Total Surface Conc., $\mu m^2\ cm^{-3}$	Examined T Range, °C	Examined RH_{ice} Range, %	Evaluated n_s, m^{-2}	T (Evaluated n_s), °C	RH_{ice} (Evaluated n_s), %
HALO05_24	200	115.0	14.4	−76.1 to −81.9	100.6 to 164.8	10^{11}	−78.2	136.4
HALO04_09	500	112.5	26.9	−75.8 to −80.1	100.3 to 149.8	10^{11}	−77.5	128.3
HALO04_05	500	142.2	30.9	−61.8 to −65.5	100.2 to 135.6	10^{11}	−62.6	111.1
HALO05_18	200	161.9	21.8	−60.3 to −65.2	100.1 to 124.5	10^{11}	−60.8	106.0
HALO06_22	200	145.7	19.2	−50.2 to −53.9	100.3 to 123.4	10^{11}	−50.7	106.7
HALO06_21	200	245.0	32.9	−50.3 to −53.8	100.4 to 115.8	10^{11}	−50.5	102.2
INUIT01_26	1000	342.1	749.0	−41.0 to −47.1	100.2 to 103.9	10^{10}	−41.2	102.2
HALO06_19	200	283.0	42.9	−39.7 to −44.5	100.2 to 121.6	10^{10}	−40.6	109.2
HALO06_20	200	168.7	22.4	−39.8 to −44.4	100.4 to 128.8	10^{10}	−40.7	111.3
INUIT04_08	1000	193.0	647.0	−39.3 to −45.4	100.0 to 113.2	10^{10}	−40.4	110.1
INUIT04_10	1000	161.7	546.6	−37.5 to −43.7	100.0 to 124.1	10^{10}	−40.1	123.3
INUIT01_30	1000	414.5	889.7	−34.6 to −42.0	100.2 to 127.1	2.5×10^8	−37.0	122.8

ACPD
14, 16493–16528, 2014

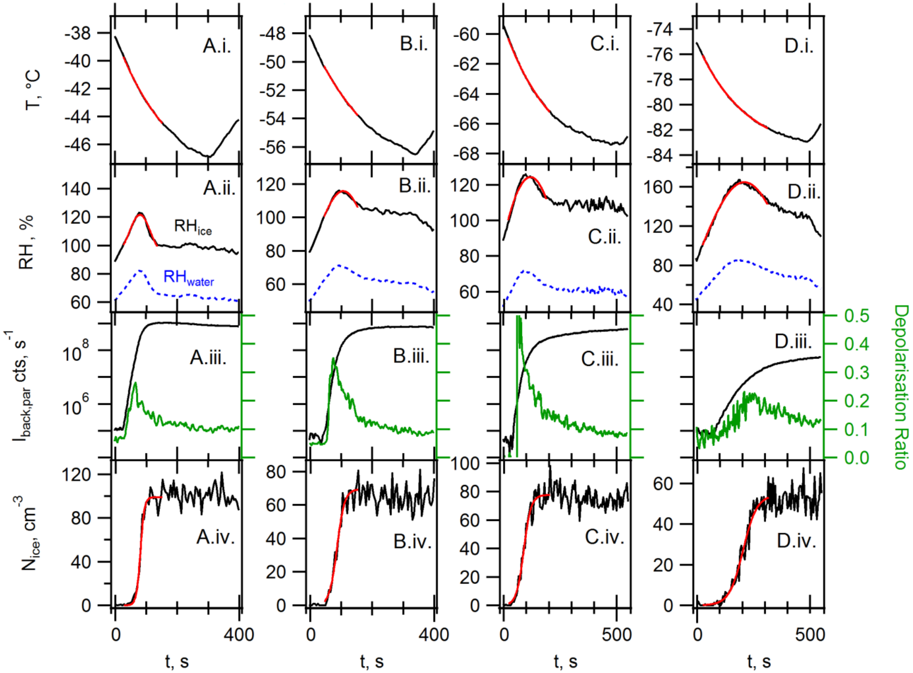

Figure 1. Temporal plots of the representative AIDA deposition mode freezing experiments with various cooling ranges including **(A)** HALO06_19, **(B)** HALO06_21, **(C)** HALO05_18 and **(D)** HALO05_24. Panels are arranged to show the measurements of i. AIDA mean gas temperature (T), ii. TDL, iii. SIMONE and iv. ice crystal concentration (N_{ice}). Note that the red lines represent interpolated data used for the n_s-isoline formulation. The $I_{back,\,par}$ in panel iv axis denotes the backscattered light scattering intensity parallel to the incident polarisation state (log-scaled). An increase in the depolarisation ratio indicates the formation and growth of ice crystals.

ACPD
14, 16493–16528, 2014

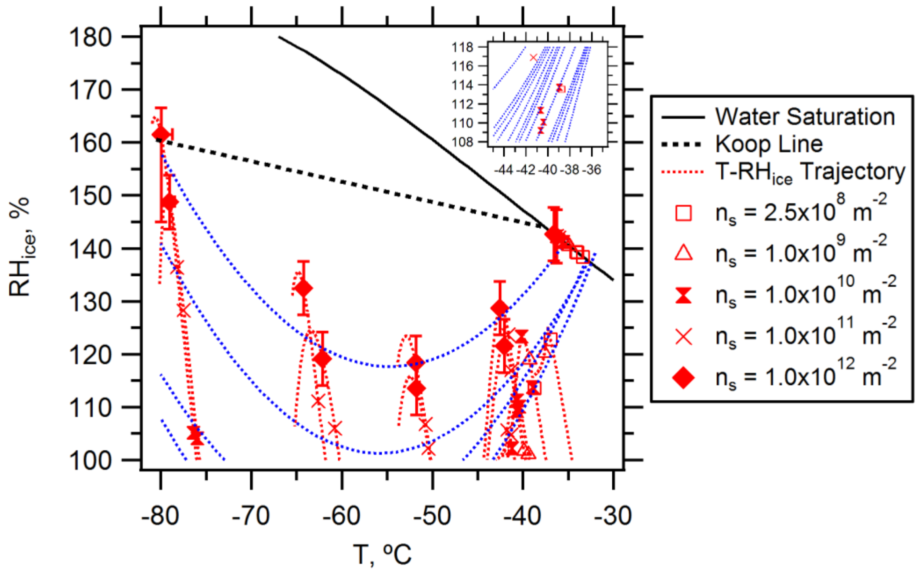

Figure 2. The constant n_s magnitudes are joined by lines (blue), representing "isolines" of hematite freezing profiles in the T-RH$_{ice}$ space. The interpolated isolines are equally spaced every order of magnitude from $10^{12}\,m^{-2}$ (top) to $10^{9}\,m^{-2}$ (bottom). Experimental trajectories of AIDA expansion-experiments with hematite particles are shown as red dotted lines. The data on the water saturation line represents the previously reported results of immersion freezing (Hiranuma et al., 2014). The sub-panel shows a magnified section of T (−35 to −45 °C) and RH$_{ice}$ (110 to 120 %) space with equi-distant n_s spacing (every quarter magnitude). The error bars at n_s of $10^{12}\,m^{-2}$ are from welas.

ACPD
14, 16493–16528, 2014

A comprehensive parameterization of heterogeneous ice nucleation of dust

N. Hiranuma et al.

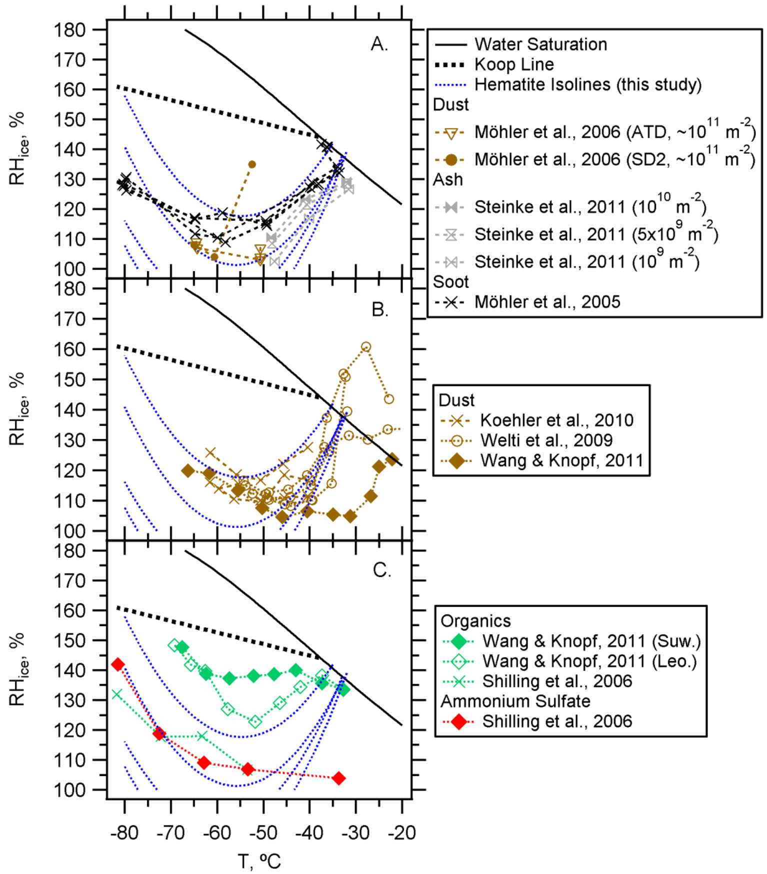

Figure 3. Ice nucleation onset T-RH$_{ice}$ of previously published data (**A** AIDA studies, **B** dust, and **C** organics and ammonium sulfate) overlaid on the isolines of hematite particles from the present study (10^{12} m^{-2}, top, to 10^{9} m^{-2}, bottom).

ACPD
14, 16493–16528, 2014

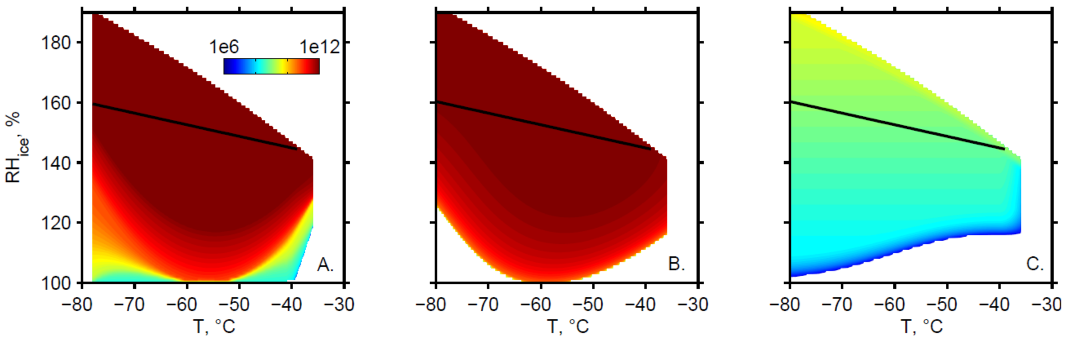

Figure 4. Spatial plot of isolines for constant n_s derived from **(A)** interpolating AIDA data, **(B)** applying third degree polynomial fit function on interpolated AIDA data and **(C)** a previously published parameterization (Phillips et al., 2013) for hematite particles. Color scale displays log-scaled n_s values in m^{-2}, applicable to all panels. The solid black lines indicate homogeneous freezing threshold line (i.e., Koop line).

ACPD
14, 16493–16528, 2014

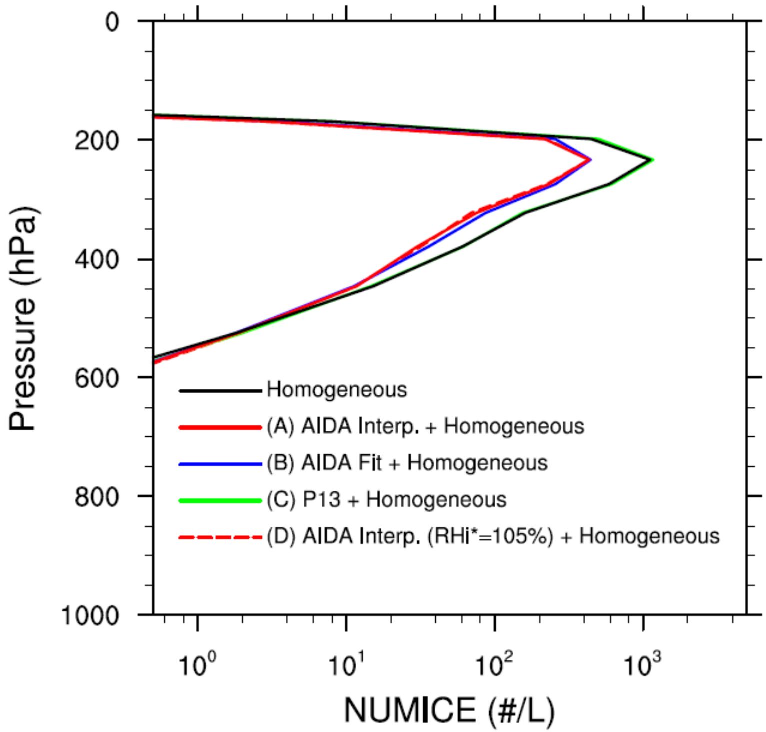

Figure 5. Monthly mean profiles of the simulated ice crystal number concentrations over the ARM SGP site. The four cases shown in the figure include the pure homogeneous ice nucleation case and three combined (heterogeneous + homogeneous) ice nucleation cases.

ACPD
14, 16493–16528, 2014

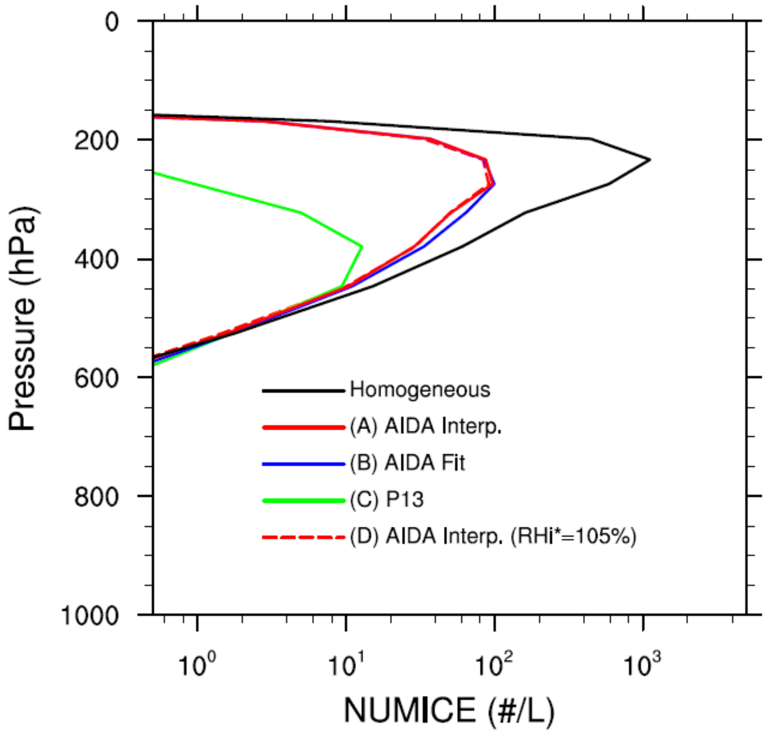

Figure 6. Monthly mean profiles of the simulated ice crystal number concentrations over the ARM SGP site. The four cases shown in the figure include the pure homogeneous ice nucleation case (HOM) and three pure heterogeneous ice nucleation cases.

ACPD
14, 16493–16528, 2014

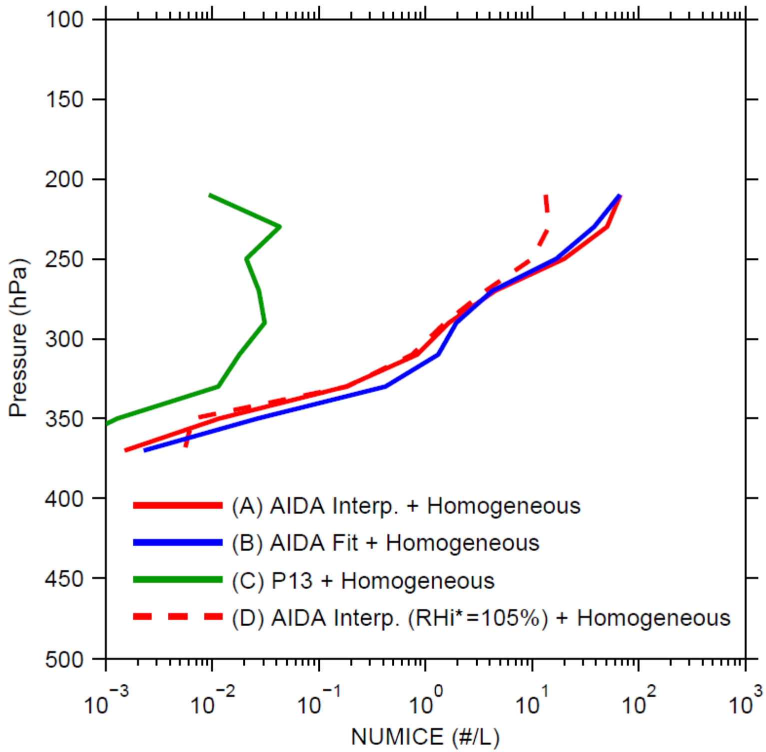

Figure 7. The mean ice number concentrations simulated in COSMO. The red dashed line represents the simulation with 105 % RH_{ice} as the lower boundary of ice formation, while others with 100 % for the minimum RH_{ice} value.

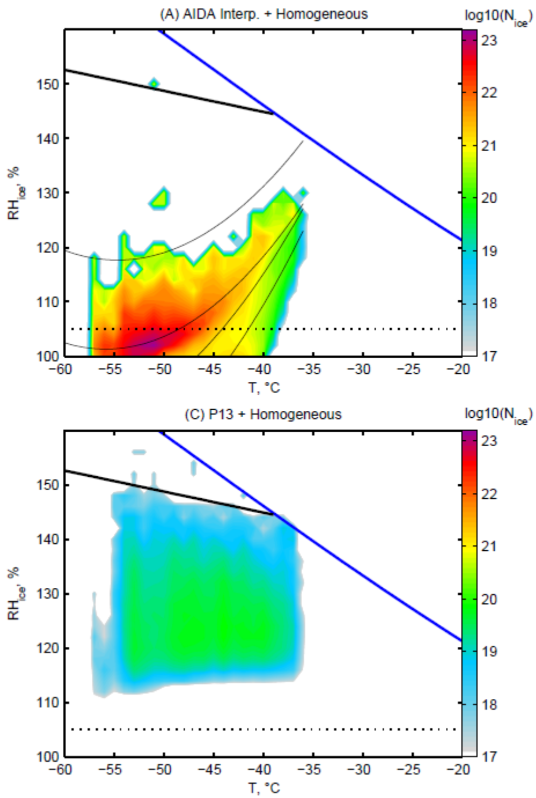

Figure 8. Accumulated ice crystal concentrations (color scale in total crystals per model domain) as a function of temperature (1 °C bins) and RH_{ice} (2 % bins). Heterogeneous nucleation simulated by AIDA parameterization (i.e., Fig. 4a) and P13 parameterization (i.e., Fig. 4c) was combined with homogeneous nucleation of cloud droplets.

ACPD
14, 16493–16528, 2014